Communications in Computational Chemistry
Commun. Comput. Chem. Vol. 8, No. 1, 54–62
doi: 10.4208/cicc.2025.340.01
Regular Article

Revisiting the Photo-Induced Paternò-Büchi Reaction Mechanism by MS-CASPT2 Method

Pengbo Gao[1], Jing Xie[1] and Quansong Li[1,*]

[1] *School of Chemistry and Chemical Engineering, Beijing Institute of Technology, Beijing, 100081, China.*

[*] Corresponding author: liquansong@bit.edu.cn.

Received 6 Dec. 2025; Accepted (in revised version) 7 Jan. 2026

Abstract: The Paternò-Büchi (P-B) reaction can generate oxetane, which is of great value in organic synthesis and medicinal chemistry, but its mechanism remains controversial. In this work, we studied the mechanism of the P-B reaction between acetone and butene to form oxetane by using the method of multistate complete active space perturbation theory (MS-CASPT2). The calculation results establish that this reaction can occur on both singlet potential energy surfaces involving the S_0 and S_1 ($^1n\pi^*$) states, as well as on triplet potential energy surfaces containing the $^3n\pi^*$ and $^3\pi\pi^*$ states. The reaction pathways on both singlet and triplet states are energetically allowed. For the C-O attack pathway, there exist significant differences in structure and energy between the conical intersection point $(S_1/S_0)_x$-1 on the singlet reaction path and the intermediate $^3I_{CO}$ on the triplet reaction path. For the C-C attack pathway, the conical intersection point $(S_1/S_0)_x$-2 and the triplet intermediate $^3I_{CC}$ almost coincide, which means that the singlet and the triplet reaction paths go through a region where the energies of the four states (S_1, T_2, T_1, and S_0) are approximately degenerate. Our results have provided new insights into the mechanism of the P-B reaction.

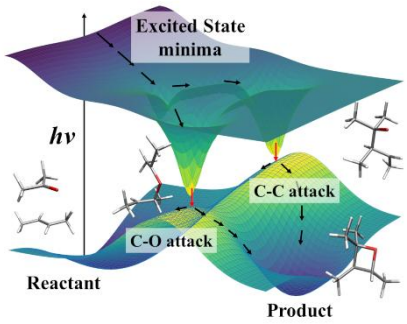

Key words: Paternò-Büchi reaction, excited state, photochemistry, conical intersection.

1. Introduction

The Paternò-Büchi (P-B) reaction, one of the [2+2] photocycloaddition reactions between a carbonyl compound and an alkene, is a flexible photochemical process that produces four-membered oxygen heterocycles oxetanes [1,2]. Oxetanes are found in the chemical structures of several natural and biologically active compounds [3], such as an antitumor drug paclitaxel [4], merrilactone possessing neurotrophic activity [5], and oxetanocin showing anti-HIV activity [6]. High regioselectivity and stereoselectivity in the P-B reaction can be obtained by proper adjusting the structures of the reactants [2]. In addition to its widespread applications in organic synthesis and medicine chemistry, the P-B reaction has significant value for locating the position of double bonds in alkenes, a topic of substantial interest in the field of lipidomics [7,8].

Although the P-B reaction has been known for more than a century [9,10], its mechanism continues to be an active area of research and debate. The mechanism of the Paternò–Büchi reaction presents several unresolved questions, including (1) Does the reaction take place in the singlet excited state (S_1 state) or the triplet excited state (T_1 state)? (2) Is the reaction concerted or stepwise? (3) Which intermediates are involved in the reaction? (4) What is the specific reaction pathway?

Early in 1954, Büchi et al. proposed that the P-B reaction of benzaldehyde with 2-methyl-2-butene involves the most stable biradical intermediate formed by the triplet-state carbonyl compound reacting with the ground-state alkene [10-12]. This triplet state-involved mechanism was supported by multiple follow-up experiments [13-17] and calculations [18-20]. However, Turro et al. studied the P-B reaction between acetone and the trans-dicyanoethylene (t-DCE) and found this photocycloaddition does not proceed via the acetone triplet state but via a singlet complex of acetone and t-DCE [21,22]. Further investigation of Turro and Wriede on the photocycloaddition of acetone to 1-methoxy-l-butene revealed that both acetone singlets and acetone triplets are involved in oxetane formation based on kinetic analysis and quantum yield studies [23]. Robb and co-workers performed MC-SCF calculations on the P-B reaction between formaldehyde and ethylene and revealed the C-O attack and C-C attack pathways behave differently [24]. For the singlet reaction the C-C attack pathway is favored and it is concerted, while the C-O attack pathway is stepwise due to the S_0/S_1 conical intersection that located before the formation of the biradical intermediate. They also found the triplet biradicals have similar energies and structures to the singlets,

and the triplet reaction pathways can be predicted by the most stable biradical rule [24]. The biradical intermediates in the P–B reaction of formaldehyde and ethylene were evaluated in view of the spin-orbital coupling (SOC) between the singlet and triplet states. The computed SOC value in the C-C attack course is two orders of magnitude larger than that in the C–O attack, indicating the C-C attack path is more possible [25]. Meanwhile, exploring the P-B reaction pathways of $H_2CO+C_2H_4$ with artificial force induced reaction (AFIR) method showed that the C–O–C–C biradical formation by C-O attack is more favorable than the O–C–C–C biradical formation by C-C attack [26]. Transient electronic and vibrational absorption spectroscopies on the photo-induced P−B reaction between benzaldehyde and cyclohexene also provided the evidence on the T_1 state of benzaldehyde that decays at a timescale of 80 ps through reaction with cyclohexene and the C−O bond formation to the biradical intermediate [27]. Conformational analysis of singlet-triplet state mixing in P-B radicals with MP2 and MCSCF methods by Kutateladze [28] supported the Griebeck model of ISC-controlled stereochemistry of P-B reactions [29]. In case of P-B reactions with electron-rich alkenes, photo-induced electron transfer (PET) from the alkenes to carbonyl compounds may occur, leading to the formation of radical-ion pair [30,31]. Frequently, P-B reactions involving a PET mechanism are more selective than those only via a biradical intermediate [32]. It is worth mentioning that most P-B reactions take place through the interaction of the excited-state carbonyl compounds with the ground-state alkenes, but the transposed P-B reaction was also obtainable where the excited-state alkene reacts with a ground-state carbonyl compound [33].

Given the significant importance of the P-B reaction and the debates surrounding its mechanism, we employed the MS-CASPT2 method in this study to investigate the mechanism of oxetane formation from the P-B reaction model system acetone and trans-butene under light irradiation (see **Scheme 1**). Both C-O attack and C-C attack pathways in singlet and triplet states were considered.

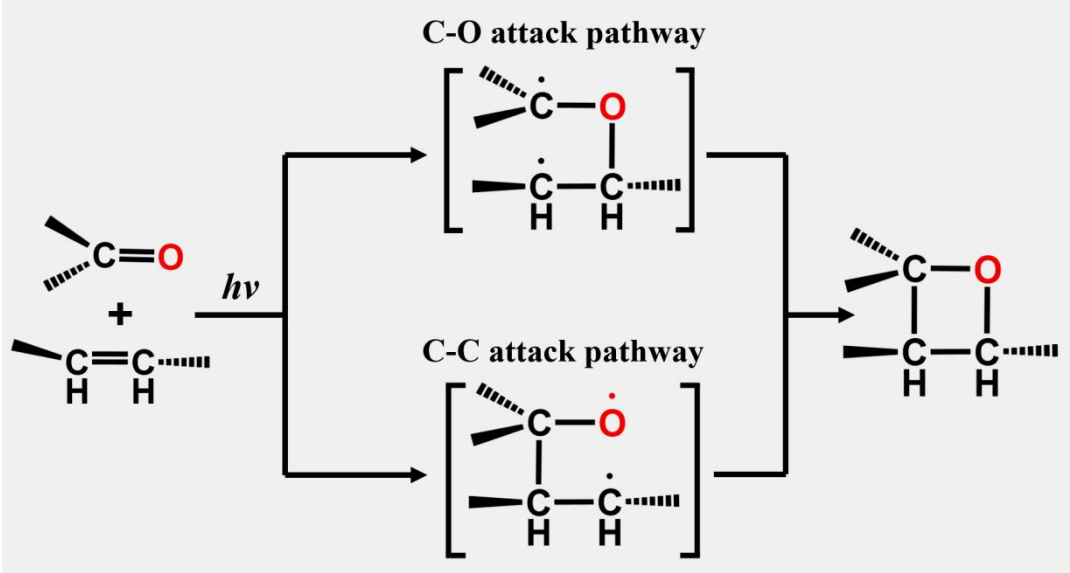

Scheme 1. Schematic diagram of the photoinduced P-B reaction between acetone and trans-butene.

2. Computational details

All the critical points (minima, transition states (TSs) and conical intersections (CIs)) and reaction pathways in this work were calculated by the MS-CASPT2 [34] method with the ANO-S-VDZP basis set [35]. On top of the optimized geometries vibrational frequencies were computed at the same theoretical level to confirm that the obtained structures were true minima or first-order saddle points. The intrinsic reaction coordinate (IRC) method [36,37] was used to search the two critical points connected by the TS, and the linear interpolation approach or constrained optimization was employed to explore the decay pathways that pass the intersection points. The decay pathways from the Franck-Condon point to the excited-state minima were traced with the minimum energy path (MEP) method. In MS-CASPT2 single-point calculations, five roots were computed with equal weights. An imaginary level shift [38] parameter of 0.2 a. u. and no ionization potential-electron affinity (IPEA) [39] were used. The spin-orbital coupling (SOC) strength between singlet and triplet states was calculated with atomic mean-field integrals by using one-electron operator.

The choice of orbitals in the active space is a key step in MS-CASPT2 calculations [40]. To keep line with previous computational studies [24,26,41] on the mechanism of the Paternò-Büchi reaction in model systems, we chose the (6,5) active space in this work. As shown in **Figure 1**, the (6,5) active space for the Franck-Condon (FC) structure of the reactant (acetone-butene complex) contains two pairs of π/π^* orbitals locating on the C=O and C=C bonds and one in-plane non-bonding orbital of the oxygen atom.

To validate the choice of the active space, we performed TD-DFT calculations employing the B3LYP [42] and CAM-B3LYP [43] functionals with the 6-311+g(d,p) basis set [44,45]. The empirical D3 dispersion corrections [46] with the Becke-Johnson damping potential [47] were used to describe the weak interactions. The MS-CASPT2 calculations were performed with the OpenMolcas v25.06 software [48] and the TD-DFT calculations were performed with the Gaussian 16 software [49].

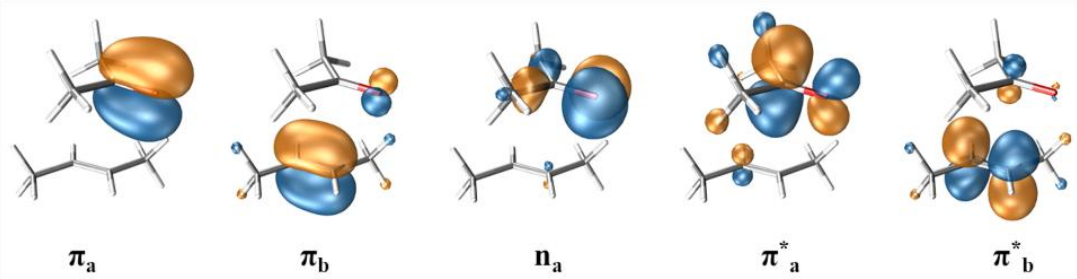

Figure 1. Active orbitals used for the calculations at the Franck-Condon structure of the reactant (^{1}R) in this work.

3. Results

3.1 Ground-state equilibrium structures and vertical excitations

Figure 2 displays the optimized structures of acetone, butene, and the acetone-butene complex (denoted as ^{1}R) in their ground states. Energies and Cartesian coordinates of all the optimized structures in this work are given in the supporting information. MS-CASPT2 method predicted the C=O bond in acetone to be 1.23 Å long and the C=C bond in butene to be 1.36 Å long, which are 0.02 Å and 0.03 Å longer than the corresponding values predicted by B3LYP and CAM-B3LYP methods. In ^{1}R, the C=O and C=C bonds align parallelly and maintain the length as in the isolated acetone and butene molecules. And the intermolecular distances are 3.28 Å for O1-C6 and 3.55 Å for C2-C7,indicating a very weak intermolecular interaction.

The vertical excitation energies, oscillator strengths, and dominant configurations of the reactant were computed using the MS-CASPT2 method and are shown in **Table 1**. For comparison, the TD-B3LYP and TD-CAM-B3LYP vertical excitations at the ^{1}R structure and the MS-CASPT2 results for isolated acetone and butene molecules are given in **Table SI-2** to **Table SI-5**. The S_1 state of ^{1}R is an nπ* state of the C=O site located at 4.31 eV (288 nm) above the FC point and is an almost dark state with an oscillator strength of 6.76×10^{-6}. The nature and energy of this S_1 state match well the S_1 state of the isolated acetone in **Table SI-4**. The S_2 state of the ^{1}R structure is a charge transfer (CT) state originating from the excitation of an electron from the π orbital of the C=C bond to the π* orbital of the C=O bond. The S_2 state has an oscillator strength of 7.33×10^{-5} and an energy of 6.76 eV with respect to that of ^{1}R. According to the computed energetics, the excitation light of 254 nm (4.88 eV) usually used in P-B experiments [50] can only populate the S_1 state of our model system.

As for the low-lying triplet states, the T_1 state lies 0.3 eV below the S_1 state and has typical nπ* character, corresponding to one-electron transition from the n orbital of the acetone oxygen atom to the π* orbital of the C=O bond. The T_2 state is of typical ππ* character, arising from one-electron transition from the π bonding orbital to the π* antibonding orbital of the C=C bond in butene. Notably, the T_2 state energy lies close to that of the S_1 state. The S_1-T_2 energy difference was predicted to -0.05, 0.35, 0.50 eV by MS-CASPT2, TD-B3LYP, and TD-CAM-B3LYP method, respectively. The above discrepancies can be mainly attributed to the different calculation methods. The MS-CASPT2 method can accurately describe dynamic electron correlation effects in multi-reference systems, but the number of orbitals in the active space is limited. The excitation energies obtained by the TD-DFT method are highly dependent on the employed functionals. Moreover, the SOC value between S_1 state and T_2 state is 1.28 cm^{-1} as computed by the MS-CASPT2 method. Given both small energy difference and non-negligible SOC between S_1 state and T_2 state, the intersystem crossing (ISC) from the S_1 state to the T_2 state cannot be ruled out for the studied model system, especially in the presence of sensitizers. This is consistent with reported transposed P-B reactions between phenyl ketone and some enamides under sensitized irradiation conditions [33].

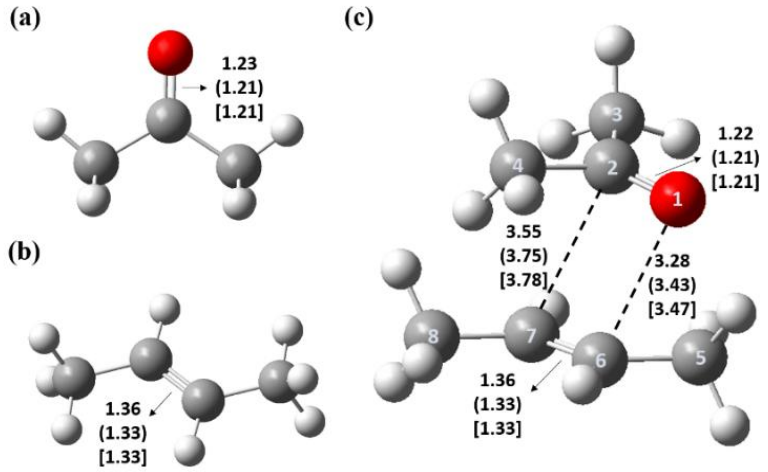

Figure 2. Optimized ground-state structures and selected distances (in Å) of (a) acetone, (b) butene, and (c) acetone-butene complex (^{1}R) by MS-CASPT2, B3LYP (in parentheses), and CAM-B3LYP (in square brackets) methods. The O, C, and H atoms are indicated in red, dark grey, and light grey colors.

Table 1. Relative MS-CASPT2 vertical excitation energy (ΔE), wavelength (λ), and oscillation strength (f) at ground state structure of the reactant (^{1}R), along with the main configuration ("u" and "d" stand for singly occupied orbitals with electrons of spin up and spin down).

State	Configuration	Weight	ΔE (eV)	λ (nm)	f
S_0	22200	0.87	0.00		
T_1	22uu0	0.88	4.01	309	
S_1	22ud0	0.61	4.31	288	6.76E-06
T_2	2u20u	0.79	4.36	284	
T_3	u22u0	0.92	6.11	203	
S_2	2u2d0	0.46	6.76	183	7.33E-05
S_3	2ud20	0.36	7.98	155	1.17E-02
T_4	2uduu	0.30	8.14	152	
T_5	2uudu	0.55	8.54	145	
S_4	ud220	0.29	9.41	132	5.78E-01

3.2 Initial decay from Franck-Condon region

Light irradiation of 254 nm populates the reactant ^{1}R to S_1 state. The decay path leads to the S_1 minimum ($^1R_{n\pi^*}$) without any barrier (see **Figure SI-1**). At the structure of $^1R_{n\pi^*}$ (see **Figure 3**), the C=O bond length increases to 1.35 Å, while the C=C bond length remains 1.36 Å, identical to its value in the ^{1}R structure. $^1R_{n\pi^*}$ is 3.54 eV higher in energy than ^{1}R. The T_1 state lies only 0.14 eV below the S_1 state and the SOC value between S_1 and T_1 states is 0.47 cm^{-1} at this $^1R_{n\pi^*}$ structure, so intersystem crossing from S_1 to T_1 state is possible, albeit with low probability. Around $^1R_{n\pi^*}$, the triplet $n\pi^*$ minimum ($^3R_{n\pi^*}$) was located (**Figure 3**), lying 0.14 eV lower in energy than $^1R_{n\pi^*}$. The structure of $^3R_{n\pi^*}$ (in which the C=O bond length is 1.34 Å) is close to $^1R_{n\pi^*}$ as well.

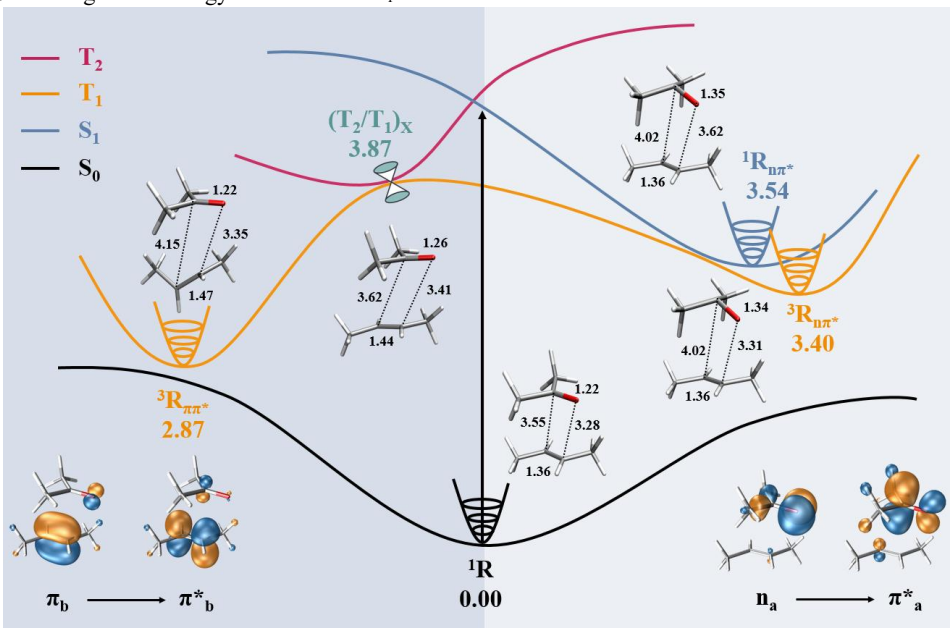

Figure 3. MS-CASPT2 energy profile (energy in eV) with key structures (distances in Å) for the initial decay of acetone and butene from Franck-Condon region.

Additionally, we noticed that the MS-CASPT2 energies of S_1 (4.31 eV), T_2 (4.36 eV), and T_1 (4.01 eV) states are close in the Franck-Condon region and tried to optimize the intersection points among these three states. A conical intersection point between T_2 state and T_1 state was obtained, labeled as $(T_2/T_1)_X$, with an energy of 3.87 eV. At the structure of $(T_2/T_1)_X$ (**Figure 3**), the C=O bond increases by 0.04 Å and the C=C bond increases by 0.08 Å compared with those in the ^{1}R structure. Inspection of the involved orbitals at $(T_2/T_1)_X$ in **Table SI-6** clearly shows that the two triplet states are the $^3n\pi^*$ state of the C=O bond in acetone (T_1 state) and the $^3\pi\pi^*$ state of the C=C bond in butene (T_2 state). **Figure 4** shows the energy profiles of

the S_1, T_2, and T_1 states together with the SOC values between the S_1 state and the two triplet states from ^1R to $(T_2/T_1)x$ along the interpolation coordinate. It can be seen that the three states (S_1, T_2, and T_1) are close in energy in this region. The SOC values between S_1 state and T_2 state are much larger than those between S_1 state and T_1 state due to the El-Sayed rule [51]. This is because both the S_1 and T_1 states are the $^3n\pi^*$ state of the C=O bond in acetone while the T_2 state is the $^3\pi\pi^*$ state of the C=C bond in butene. Therefore, the ISC from the S_1 state to the T_2 state is more likely to occur in this nearly degenerate region. From $(T_2/T_1)_X$, the decay paths may lead to either $^3R_{n\pi^*}$ or $^3R_{\pi\pi^*}$ without any barrier (**Figure SI-2** and **Figure SI-3**). At the structure of $^3R_{\pi\pi^*}$ (**Figure 3**), the C=C bond increases to 1.47 Å and the C=O bond remains unchanged of 1.22 Å at the ^1R structure. The energy of $^3R_{\pi\pi^*}$ is 0.53 eV lower than that of the $^3R_{n\pi^*}$ minimum.

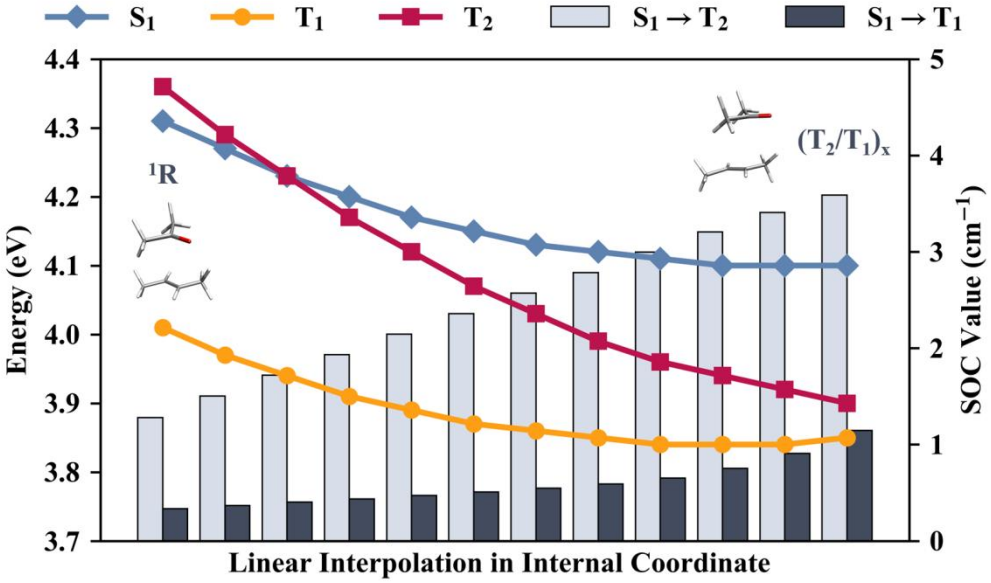

Figure 4. Potential energy profile of S_1, T_2, and T_1 states from the Franck-Condon point ^1R to the intersection point $(T_2/T_1)x$. The bar graph shows the SOC values between the S_1 state and two triplet states.

3.3 Reaction pathways from the S_1 minimum

Inspired by the pioneering work on the P-B reaction mechanism for formaldehyde and ethylene by Robb et al. [24], we investigated the P-B reaction mechanism of our system in singlet state via both C-O attack and C-C attack pathway. The obtained MS-CASPT2 energy profiles are shown in **Figure 5**.

For the C-O attack, the reaction pathway was computed along the C6-O1 coordinate with the C6-O1 distance ranging from 3.62 Å at $^1R_{n\pi^*}$ to 1.65 Å at the conical intersection point between S_1 state and S_0 state labelled as $(S_1/S_0)_x$-1 hereafter. The MS-CASPT2 energy profile from $^1R_{n\pi^*}$ to $(S_1/S_0)_x$-1 (**Figure SI-4**) shows that this pathway has an energy barrier of approximately 0.44 eV. However, the 254 nm (4.88 eV) excitation light provides sufficient energy to overcome this barrier. At the structure of $(S_1/S_0)_x$-1, the C6-O1 bond almost forms, as the distance of 1.65 Å is only slightly longer than a typical C-O single bond (ca.1.5 Å). From $(S_1/S_0)_x$-1, the decay pathway may lead to the ground-state oxetane product ^1P by overcoming a barrier of about 0.35 eV, or go back to the ground-state reactant ^1R without any barrier (see **Figure SI-5** and **Figure SI-6**). At the structure of ^1P, the four-membered oxetane ring is formed. The C-O bond lengths (1.45 Å and 1.46 Å) are approximately 0.1 Å shorter than the C-C bond lengths (1.54 Å and 1.56 Å). In terms of energy, ^1P lies 0.07 eV below ^1R.

Regarding the C-C attack, the reaction pathways (see **Figure 5**) are similar to those of the C-O attack, but with two notable differences. One difference is that the S_1/S_0 conical intersection point for the C-C attack, $(S_1/S_0)_x$-2, is 0.65 eV lower than $(S_1/S_0)_x$-1 for the C-O attack. The other difference is that all the decay pathways related with $(S_1/S_0)_x$-2 are barrierless, including the pathway from $^1R_{n\pi^*}$ to $(S_1/S_0)_x$-2 in **Figure SI-7** and the pathways from $(S_1/S_0)_x$-2 to ^1P and ^1R in **Figure SI-8** and **Figure SI-9**. The C2-C7 distance of 1.58 Å at $(S_1/S_0)_x$-2 is very close to that of 1.56 Å at ^1P.

3.4 Reaction pathways from the triplet minima

The $^3n\pi^*$ state of the carbonyl group is generally accepted to take part in the photochemical P-B reactions [17]. **Figure 6** shows the reaction pathways from the $^3R_{n\pi^*}$ minimum of our studied system. For the C-O attack, we located a transition state ^{3}TS-1, which connects $^3R_{n\pi^*}$ and the biradical triplet minimum $^3I_{CO}$ by overcoming a small energy barrier of 0.12 eV (see **Figure SI-10** for the IRC energy profile). At ^{3}TS-1, the C6-O1 distance is 2.20 Å , which decreases to 1.47 Å at $^3I_{CO}$. Concurrently, the C2-O1 bond changes from 1.34 Å to 1.30 Å, and the C6-C7 bond in butene increases from 1.38 Å to 1.46 Å. These structure changes indicate the formation of C6-O1 bond forms and the conversion of the C6=C7 double bond to a single bond upon biradical formation. Notably, at $^3I_{CO}$, the S_0 state is only 0.03 eV below the T_1 state, and the SOC value between the T_1 and S_0 states is 0.462 cm^{-1}. These conditions suggest that ISC from the T_1 state to the S_0 state is feasible. Once the system is populated in the S_0 state of the intermediate, the decay pathways may go further to the product ^1P or the reactant ^1R without any barriers (see the energy profiles in **Figure SI-11** and **Figure SI-12** by fixed optimizations).

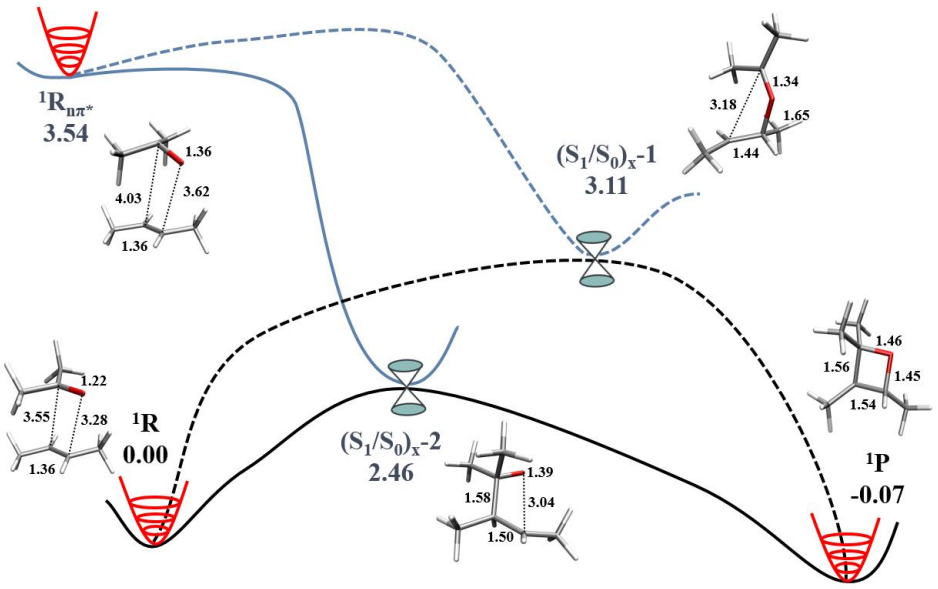

Figure 5. MS-CASPT2 energy profile (energy in eV) with key structures (distances in Å) for the studied P-B reaction in singlet states. The blue lines are for the S_1 state and the black lines are for S_0 state.

The C-C attack pathway from the $^3R_{n\pi^*}$ minimum is quite similar to that of the C-O attack. The optimized transition state ^{3}TS-2 for the C-C attack pathway lies 0.08 eV above the reactant $^3R_{n\pi^*}$. After passing through ^{3}TS-2, the system relaxes to a triplet minimum point $^3I_{CC}$ (see **Figure SI-13** for the IRC energy profile). Interestingly, at $^3I_{CC}$, the C=O bond in acetone and the C=C bond in butene stretched to 1.39 Å and 1.50 Å, which are identical to their respective lengths at $^3I_{CO}$. The newly formed C2-C7 bond at $^3I_{CC}$ has a length of 1.56 Å, exhibiting typical character of a C-C single bond. The energy difference between the T_1 and S_0 states at the structure of $^3I_{CC}$ is 0.08 eV and the SOC value between these two states is 11.1 cm^{-1}, allowing ISC from the T_1 state to the S_0 state. Subsequently, the decay pathways from $^3I_{CC}$ on the S_0 surface to both ^{1}P and ^{1}R are barrierless (see **Figure SI-14** and **Figure SI-15** for the energy profiles).

In addition, it was found that the two triplet intermediates $^3I_{CC}$ and $^3I_{CO}$ are connected by a transition state point ^{3}TS-3. The structure and energy of ^{3}TS-3 are provided in **Figure 6**, and the IRC energy profile from ^{3}TS-3 is shown in **Figure SI-16**. At ^{3}TS-3, the C2-C7 distance is 2.41 Å and the O1-C6 separation is 1.99 Å. These values are intermediate between the corresponding distances in the structures of $^3I_{CO}$ and $^3I_{CC}$. However, the energy barrier along this reaction pathway is close to 0.8 eV, suggesting that the interconversion between $^3I_{CC}$ and $^3I_{CO}$ is unlikely to occur.

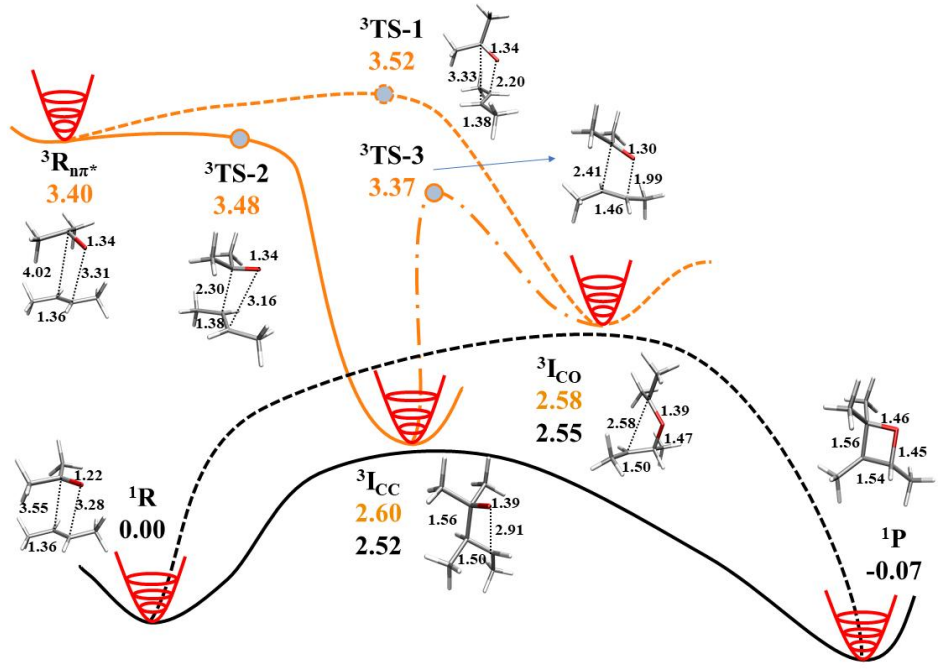

Figure 6. MS-CASPT2 energy profile (energy in eV) with key structures (distances in Å) for the studied P-B reaction from the $^3R_{n\pi^*}$ minimum. The orange line represents the triplet state, and the black line is for the S_0 state.

Figure 7. MS-CASPT2 energy profile (energy in eV) with key structures (distance in Å) for the studied P-B reaction from the $^3R_{\pi\pi^*}$ minimum. Upon reaching the biradical intermediates ($^3I_{cc}$ and $^3I_{co}$), the subsequent reaction pathways are consistent with those in **Figure 6**.

From the $^3R_{\pi\pi^*}$ minimum, we also explored the possible reaction pathways leading to the oxetane product. The optimization for the C-C attack yielded a transition state ^{3}TS-4 (see **Figure 7**), where the C2-C7 distance is 1.97 Å and the C6-C7 bond length is 1.48 Å. IRC energy profile in **Figure SI-17** confirms that ^{3}TS-4 connects the $^3R_{\pi\pi^*}$ minimum and $^3I_{CC}$. The energy of ^{3}TS-4 is 0.31 eV higher than that of the $^3R_{\pi\pi^*}$ minimum, suggesting that the formation of $^3I_{CC}$ from $^3R_{\pi\pi^*}$ minimum is energetically allowed. In the C-O attack direction, optimization for the transition state resulted in a second-order saddle point ^{3}TS-5 (see **Figure 7**) with two imaginary frequencies of -489 cm^{-1} and -68 cm^{-1}. Since the energy of ^{3}TS-5 is 0.78 eV higher than that of the $^3R_{\pi\pi^*}$ minimum, the reaction pathway via ^{3}TS-5 can be ruled out.

4. Discussion

According to our potential energy surface calculations, the mechanism of the studied P-B reaction between acetone and butene is summarized in **Scheme 2**. Photoexcitation at 254 nm populates the S_1 state of the reactant ($^1R_{n\pi^*}$), which is the nπ* state of the C=O site in acetone. In the S_1 state, the reaction pathways may lead to the ground-state product ^{1}P via conical intersection points $(S_1/S_0)_x$ between the S_1 state and the S_0 state. In addition, the two triplet states ($^3R_{n\pi^*}$ and $^3R_{\pi\pi^*}$) can be populated from the S_1 state by intersystem crossing owing to the small energy difference and the nontrivial spin-orbital couplings between the S_1 state and the triplet states. From the $^3R_{n\pi^*}$ minimum, there exist two different pathways to ^{1}P. One path first goes to the $^3I_{CO}$ intermediate along the C-O attack direction, followed by the C-C bond formation to complete the oxetane ring. The other path first leads to the $^3I_{CC}$ intermediate along the C-C attack direction, then the C-O bond comes to formation. From the $^3R_{\pi\pi^*}$ minimum, there is only one pathway via $^3I_{CC}$ to ^{1}P is energetically allowed, because the reaction pathway via $^3I_{CO}$ has a high energy barrier up to 0.78 eV. Moreover, our calculations reveal that the reaction pathways may go back to the ground-state reactant ^{1}R from several sites, including $^3R_{\pi\pi^*}$, $^3I_{CO}$, $^3I_{CC}$, and the conical intersections. These at least partially explains why the yield of P-B reaction was observed to be relatively low in some experiments [12].

Our MS-CASPT2 calculations reveal that in the P-B reaction between acetone and butene, potential energy surface crossings are not only widespread but also determine many key steps, including the intersystem crossings from $^1R_{n\pi^*}$ to $^3R_{n\pi^*}$ and $^3R_{\pi\pi^*}$, the decays through $(S_1/S_0)_x$-1 and $(S_1/S_0)_x$-2 on the singlet reaction pathways, and the return of triplet intermediates $^3I_{CO}$ and $^3I_{CC}$ to the S_0 state ultimately leading to the formation of ground-state product ^{1}P. These align with the theoretical findings in the P-B reaction between formaldehyde and ethylene, including but not limited to the important roles of $(S_1/S_0)_x$ conical intersections revealed by Robb et al. using the CASSCF method [24] and the significant contributions of the $(S_1/T_1)_x$ seam in intersystem crossing and reaction mechanism discovered by Morokuma et al. employing the AFIR method [26]. Recent theoretical study on the mechanism of Cu-catalyzed [2+2] photocycloaddition of norbornene and acetone to oxetane also revealed the crucial roles of the minimum-energy crossing points in the reaction [52].

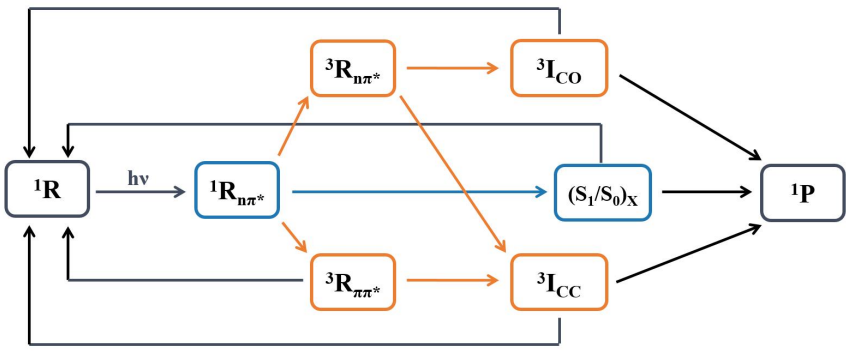

Scheme 2. Overview of the reaction pathways obtained in this work.

Interestingly, we found that for the C-O attack, there are significant differences in structure and energy between the conical intersection point $(S_1/S_0)_x$-1 on the singlet reaction path and the intermediate $^3I_{CO}$ on the triplet reaction path. Meanwhile, for the C-C attack, the $(S_1/S_0)_x$-2 on the singlet reaction path and the $^3I_{CC}$ on the triplet reaction path have similar structures and energies. This means that the singlet and triplet reaction paths of C-C attack intersect in a region where the energies of the four states $S_1/T_2/T_1/S_0$ are close to degeneracy, while this is not the case for C-O attack.

In addition, our calculation results support the widely recognized $n\pi^*$ state located in the C=O part for the excited state that triggers the P-B reaction, but also suggest that the $\pi\pi^*$ state in the C=C part may likewise be involved. This to some extent confirms the reported inverted P-B reaction in the experiment [33], although our model system is different from the real system in the experiment.

5. Conclusion

In the present work, the mechanism of the P-B reaction between acetone and butene to achieve oxetane has been investigated on the basis of the calculated potential energy surfaces (S_0, $^1n\pi^*$, $^3n\pi^*$, and $^3\pi\pi^*$ states) and their intersections. We found that the $(S_1/S_0)_x$ conical intersections play important roles in the reaction pathways of singlet states, while the $(T_1/S_1)_x$ and $(T_1/S_0)_x$ intersections facilitate the intersystem crossings involving triplet states. The photo-induced P-B reaction was found to proceed concertedly in singlet states, while in a stepwise way involving triplet states via the C-O attack ($^3I_{CO}$) or C-C attack ($^3I_{CC}$) intermediate. We have provided computational evidence on that besides the well-known $^3n\pi^*$ state of the carbonyl groups the $^3\pi\pi^*$ state of the alkene can also take part in the P-B reaction. Our results are expected to deepen the mechanism understanding of the P-B reaction. Calculations to clarify the acceleration effect of microdroplets in the P-B reaction [53] are currently under way.

Supporting Information

Supporting information can be downloaded here.

Acknowledgments

This work was supported by the National Natural Science Foundation of China (22573006) and the National Key Research and Development Program of China (2024YFA1509600). This paper is dedicated to professor Wei-Hai Fang on the occasion of his 70th birthday.

References

[1] Fréneau M. and Hoffmann N., The Paternò–Büchi reaction—mechanisms and application to organic synthesis. *J. Photochem. Photobiol. C,* **33** (2017), 83–108.

[2] D'Auria M., The Paternò–Büchi reaction – a comprehensive review. *Photochem. Photobiol. Sci.,* **18** (2019), 2297–2362.

[3] Bull J.A., Croft R.A., Davis O.A., et al., Oxetanes: recent advances in synthesis, reactivity, and medicinal chemistry. *Chem. Rev.,* **116** (2016), 12150–12233.

[4] Wani M.C., Taylor H.L., Wall M.E., et al., Plant antitumor agents. VI. Isolation and structure of taxol, a novel antileukemic and antitumor agent from taxus brevifolia. *J. Am. Chem. Soc.,* **93** (1971), 2325–2327.

[5] Huang J., Yokoyama R., Yang C., et al., Merrilactone a, a novel neurotrophic sesquiterpene dilactone from illicium merrillianum. *Tetrahedron Lett.,* **41** (2000), 6111–6114.

[6] Hoshino H., Shimizu N., Shimada N., et al., Inhibition of infectivity of human immunodeficiency virus by oxetanocin. *J. Antibiot.,* **40** (1987), 1077–1078.

[7] Ma X. and Xia Y., Pinpointing double bonds in lipids by Paternò–Büchi reactions and mass spectrometry. *Angew. Chem. Int. Ed.,* **53** (2014), 2592–2596.

[8] Zhao X., Shi H., Lin Q., et al., Review: deep lipidomic profiling enabled by the Paternò–Büchi reaction – pinpointing C C locations and beyond. *Anal. Chim. Acta,* **1376** (2025), 344456.

[9] Paternò E. and Chieffi G., Synthesis in organic chemistry using light. Note II. Compounds of unsaturated hydrocarbons with aldehydes and ketones. *Gazz. Chim. Ital.,* **39** (1909), 341–361.

[10] Büchi G., Inman C.G. and Lipinsky E.S., Light-catalyzed organic reactions. I. The reaction of carbonyl compounds with 2-methyl-2-butene in the presence of ultraviolet light. *J. Am. Chem. Soc.,* **76** (1954), 4327–4331.

[11] Büchi G., Kofron J.T., Koller E., et al., Light catalyzed organic reactions. V.1 the addition of aromatic carbonyl compounds to a disubstituted acetylene. *J. Am. Chem. Soc.,* **78** (1956), 876–877.

[12] Zimmerman H.E., Interpretation of some organic photochemistry. *Science,* **153** (1966), 837–844.

[13] Yang N.C., Nussim M., Jorgenson M.J., et al., Photochemical reactions of carbonyl compounds in solution the Paternò–Büchi reaction. *Tetrahedron Lett.,* **5** (1964), 3657–3664.

[14] Arnold D.R. and Glick A.H., The photocycloaddition of carbonyl compounds to allenes. *Chem. Commun.,* **22** (1966), 813–814.

[15] Yang N.-Chu., Loeschen R.L. and Mitchell D., Mechanism of the Paternò–Büchi reaction. *J. Am. Chem. Soc.,* **89** (1967), 5465–5466.

[16] Freilich S.C. and Peters K.S., Observation of the 1,4 biradical in the Paternò–Büchi reaction. *J. Am. Chem. Soc.,* **103** (1981), 6255–6257.

[17] Brogaard R.Y., Schalk O., Boguslavskiy A.E., et al., The Paternò–Büchi reaction: importance of triplet states in the excited-state reaction pathway. *Phys. Chem. Chem. Phys.,* **14** (2012), 8572–8580.

[18] Bunce N.J., Ridley J.E. and Zerner M.C., On the excited states of p-quinones and an interpretation of the photocycloaddition of p-quinones to alkenes. *Theor. Chim. Acta,* **45** (1977), 283–300.

[19] Pintér B., De Proft F., Veszprémi T., et al., Regioselectivity in the [2 + 2] cyclo-addition reaction of triplet carbonyl compounds to substituted alkenes (Paterno-Büchi reaction): a spin-polarized conceptual DFT approach. *J. Chem. Sci.,* **117** (2005), 561–571.

[20] D'Annibale A., D'Auria M., Prati F., et al., Paternò–Büchi reaction versus hydrogen abstraction in the photochemical reactivity of alkenyl boronates with benzophenone. *Tetrahedron,* **69** (2013), 3782–3795.

[21] Turro N.J., Wriede P.A., Dalton J.C., et al., Molecular photochemistry. V. Photocycloaddition of alkyl ketones to electron-deficient double bonds. *J. Am. Chem. Soc.,* **89** (1967), 3950–3952.

[22] Turro N.J., Wriede P.A. and Dalton J.C., Molecular photochemistry. VIII. Evidence for a singlet-state complex in the photocycloaddition of acetone to trans-1,2-dicyanoethylene. *J. Am. Chem. Soc.,* **90** (1968), 3274–3275.

[23] Dalton J.C., Wriede P.A. and Turro N.J., Molecular photochemistry. XXIV. Photocycloaddition of acetone to 1,2-dicyanoethylene. *J. Am. Chem. Soc.,* **92** (1970), 1318–1326.

[24] Palmer I.J., Ragazos I.N., Bernardi F., et al., An MC-SCF study of the (photochemical) Paternò–Büchi reaction. *J. Am. Chem. Soc.,* **116** (1994), 2121–2132.

[25] Minaev B.F. and Ågren H., Spin–orbit coupling in oxygen containing diradicals. *J. Mol. Struct. THEOCHEM,* **434** (1998), 193–206.

[26] Maeda S., Taketsugu T. and Morokuma K., Exploring pathways of photoaddition reactions by artificial force induced reaction method: a case study on the Paternò–Büchi reaction. *Z. Phys. Chem.,* **227** (2013), 1421–1433.

[27] Harris S.J., Murdock D., Grubb M.P., et al., Tracking a Paternò–Büchi reaction in real time using transient electronic and vibrational spectroscopies. *J. Phys. Chem. A,* **118** (2014), 10240–10245.

[28] Kutateladze A.G., Conformational analysis of singlet−triplet state mixing in Paternò–Büchi diradicals. *J. Am. Chem. Soc.,* **123** (2001), 9279–9282.

[29] Abe M., Torii E. and Nojima M., Paternò–Büchi photocyclization of 2-siloxyfurans and carbonyl compounds. Notable substituent and carbonyl (aldehyde vs ketone and singlet- vs triplet-excited state) effects on the regioselectivity (double-bond selection) in the formation of bicyclic exo-oxetanes. *J. Org. Chem.,* **65** (2000), 3426–3431.

[30] Gersdorf J., Mattay J. and Goerner H., Radical cations. 3. Photoreactions of biacetyl, benzophenone, and benzil with electron-rich alkenes. *J. Am. Chem. Soc.,* **109** (1987), 1203–1209.

[31] Mattay J., Gersdorf J. and Buchkremer K., Photoreactions of biacetyl with electron-rich olefins. An extended mechanism. *Chem. Ber.,* **120** (1987), 307–318.

[32] Abe M., Ikeda M., Shirodai Y., et al., Regio- and stereoselective formation of 2-siloxy-2-alkoxyoxetanes in the photoreaction of cyclic ketene silyl acetals with 2-naphthaldehyde and their transformation to aldol-type adducts. *Tetrahedron Lett.,* **37** (1996), 5901–5904.

[33] Kumarasamy E., Raghunathan R., Kandappa S.K., et al., Transposed Paternò–Büchi reaction. *J. Am. Chem. Soc.,* **139** (2017), 655–662.

[34] Finley J., Malmqvist P.-Å., Roos B.O., et al., The multi-state CASPT2 method. *Chem. Phys. Lett.,* **288** (1998), 299–306.

[35] Pierloot K., Dumez B., Widmark P.-O., et al., Density matrix averaged atomic natural orbital (ANO) basis sets for correlated molecular wave functions. *Theor. Chim. Acta,* **90** (1995), 87–114.

[36] Gonzalez C. and Schlegel H.B., An improved algorithm for reaction path following. *J. Chem. Phys.,* **90** (1989), 2154–2161.

[37] Gonzalez C. and Schlegel H.B., Reaction path following in mass-weighted internal coordinates. *J. Phys. Chem.,* **94** (1990), 5523–5527.

[38] Forsberg N. and Malmqvist P.-Å., Multiconfiguration perturbation theory with imaginary level shift. *Chem. Phys. Lett.,* **274** (1997), 196–204.

[39] Ghigo G., Roos B.O. and Malmqvist P.-Å., A modified definition of the zeroth-order Hamiltonian in multiconfigurational perturbation theory (CASPT2). *Chem. Phys. Lett.,* **396** (2004), 142–149.

[40] Veryazov V., Malmqvist P.Å. and Roos B.O., How to select active space for multiconfigurational quantum chemistry? *Int. J. Quantum Chem.,* **111** (2011), 3329–3338.

[41] Guerra C., Ayarde-Henríquez L., Duque-Noreña M., et al., Unraveling the bonding nature along the photochemically activated Paternò–Büchi reaction mechanism. *ChemPhysChem,* **22** (2021), 2342–2351.

[42] Stephens P.J., Devlin F.J., Chabalowski C.F., et al., Ab initio calculation of vibrational absorption and circular dichroism spectra using density functional force fields. *J. Phys. Chem.,* **98** (1994), 11623–11627.

[43] Yanai T., Tew D.P. and Handy N.C., A new hybrid exchange–correlation functional using the Coulomb-attenuating method (CAM-B3LYP). *Chem. Phys. Lett.,* **393** (2004), 51–57.

[44] Krishnan R., Binkley J.S., Seeger R., et al., Self-consistent molecular orbital methods. XX. A basis set for correlated wave functions. *J. Chem. Phys.,* **72** (1980), 650–654.

[45] Clark T., Chandrasekhar J., Spitznagel G.W., et al., Efficient diffuse function-augmented basis sets for anion calculations. III. The 3-21+G basis set for first-row elements, Li–F. *J. Comput. Chem.,* **4** (1983), 294–301.

[46] Grimme S., Antony J., Ehrlich S., et al., A consistent and accurate ab initio parametrization of density functional dispersion correction (DFT-D) for the 94 elements H–Pu. *J. Chem. Phys.,* **132** (2010), 154104.

[47] Becke A.D. and Johnson E.R., A density-functional model of the dispersion interaction. *J. Chem. Phys.,* **123** (2005), 154101.

[48] Li Manni G., Fdez. Galván I., Alavi A., et al., The OpenMolcas Web: a community-driven approach to advancing computational chemistry. *J. Chem. Theory Comput.,* **19** (2023), 6933–6991.

[49] Frisch M.J., Trucks G.W., Schlegel H.B., et al., Gaussian 16, Revision A.03. Gaussian Inc., Wallingford, 2016.

[50] D'Auria M. and Racioppi R., Oxetane synthesis through the Paternò–Büchi reaction. *Molecules,* **18** (2013), 11384–11428.

[51] El-Sayed M.A., Spin–orbit coupling and the radiationless processes in nitrogen heterocyclics. *J. Chem. Phys.,* **38** (1963), 2834–2838.

[52] Peng L.-Y., Jin R., Zhang S.-R., et al., Roles of nonadiabatic processes, reaction mechanism, and selectivity in Cu-catalyzed [2 + 2] photocycloaddition of norbornene and acetone to oxetane. *J. Org. Chem.,* **89** (2024), 11334–11346.

[53] Song X. and Zare R.N., The power of microdroplet photochemistry. *Chem. Sci.,* **15** (2024), 3670–3672.